

## LARGE STRAIN ELASTO-PLASTIC DYNAMIC ANALYSIS OF SHELL STRUCTURES

Yin Jaiju<sup>1</sup>, Gu Fangyu<sup>2</sup>, Liu Zishun<sup>1</sup>, Yan Wentao<sup>1</sup> and Ruan Hui<sup>2</sup>

<sup>1</sup>Xi'an Jiaotong University, Dept. of Engineering Mechanics, Xi'an,

<sup>2</sup>Nuclear Power Institute of China, Reactor Eng. Research Division, Chengdu, P.R. China

### Abstract

A refined degenerated shell element with assumed transverse shear and membrane strains is adopted. This element not only overcomes the shear and membrane locking problems but does not contain the spurious zero energy modes. In the updated Lagrangian transient dynamic formulations, the geometrically, materially nonlinear effect and large strain are considered. The nodal coordinates and the thickness of elements are updated after each time step.

Some numerical examples for elastic and elasto-plastic dynamic analysis have been given to illustrate the good numerical results.

### 1. Introduction

The original degenerated shell element performs reasonably well for moderately thick shell situations. However, for thin shell when full integration is used to evaluate the stiffness matrix, overstiff solutions are often produced due to shear and membrane locking. Attempts have been made to correct this behaviour by use of reduced or selective integration techniques [1]. Such schemes are not always successful in overcoming locking behaviour and the resulting solutions may still be overstiff for problems with highly constrained boundaries, especially when coarse meshes are used. Furthermore, for problems with lightly constrained boundaries, spurious zero energy modes may form.

Recently, the degenerated shell element has been developed [2] by using

- (1) Enhanced interpolation of the transverse shear strains in the natural coordinate system.
- (2) Enhanced interpolation of the membrane strains in the local Cartesian coordinate system.

The main advantages of the new degenerated shell element are that it does not lock and has any spurious zero energy modes and gives generally very good behaviour.

In our work, for the new degenerated shell element, the updated Lagrangian formulations are deduced and the geometrically, materially nonlinear effect and large strain are considered. Some numerical examples for transient dynamic analysis of shells are executed and good results have been shown.

### 2. New Degenerated Shell Element Formulation

Now a brief review of the new degenerated element is given.

#### 2.1 Degenerated Shell Element

Two main assumptions are used in the degeneration process from solid three dimensional element to shell element. They are

- (1) 'Normals' to the middle surface before deformation remain straight after deformation.
- (2) The normal stress component is constrained to zero in the constitutive equations.

Five degrees of freedom are specified at each nodal point, corresponding to its three displacements and the two rotations of the 'normal' at the node. The definition permits transverse shear deformation to be taken into account.

A quadratic degenerated 9-node shell element is shown in Fig. 1. The coordinates of a point within the element may be expressed as

$$\begin{bmatrix} x \\ y \\ z \end{bmatrix} = \sum_{k=1}^n N_k \begin{bmatrix} x_k \\ y_k \\ z_k \end{bmatrix}_{mid} + \sum_{k=1}^n N_k l_k \zeta / 2 \begin{bmatrix} \tilde{l}_k \\ \tilde{l}_k \\ \tilde{l}_k^2 \end{bmatrix} \quad (1)$$

Where  $n$  is the number of nodes per element;  $N_k = N_k(\xi, \eta)$  ( $k = 1, \dots, n$ ) are the element shape functions corresponding to the surface  $\zeta = \text{constant}$ ;  $h_k$  is the shell thickness at node  $k$ . The vector  $t_k$  is constructed from the nodal coordinates of the top and bottom surface at node  $k$ .

The element displacement field can be expressed as

$$\begin{bmatrix} u \\ v \\ w \end{bmatrix} = \sum_{k=1}^n N_k \begin{bmatrix} u_k \\ v_k \\ w_k \end{bmatrix} + \sum_{k=1}^n N_k h_k \zeta / 2 \begin{bmatrix} \bar{r}_k^z & -\bar{s}_k^z \\ \bar{r}_k^y & -\bar{s}_k^y \\ \bar{r}_k^x & -\bar{s}_k^x \end{bmatrix} \begin{bmatrix} \beta_{1k} \\ \beta_{2k} \end{bmatrix} \quad (2)$$

2.2 Elimination of Shear Locking

For shells, the transverse shell strain  $\gamma_{\xi\zeta}$  and  $\gamma_{\eta\zeta}$  express in the natural coordinate system  $(\xi, \eta, \zeta)$  tend towards zero for thin shells. To avoid shear locking in the new 9-node degenerated shell element, Huang and Hinton [3] replaced the shear strains by substituting shear strain of the form

$$\left. \begin{aligned} \bar{\gamma}_{\xi\zeta} &= b_1 + b_2\xi + b_3\eta + b_4\xi\eta + b_5\eta^2 + b_6\xi\eta^2 \\ \bar{\gamma}_{\eta\zeta} &= c_1 + c_2\xi + c_3\eta + c_4\xi\eta + c_5\xi^2 + c_6\xi^2\eta \end{aligned} \right\} \quad (3)$$

The substitute strain field are chosen as

$$\left. \begin{aligned} \bar{\gamma}_{\xi\zeta} &= \sum_{i=1}^3 \sum_{j=1}^2 L_j(\xi) H_i(\eta) \bar{\gamma}_{\xi\zeta}^{ij} \\ \bar{\gamma}_{\eta\zeta} &= \sum_{i=1}^3 \sum_{j=1}^2 H_i(\xi) L_j(\eta) \bar{\gamma}_{\eta\zeta}^{ij} \end{aligned} \right\} \quad (4)$$

where

$$H_1(Z) = Z(Z/b + 1)/2b, \quad H_2(Z) = 1 - (Z/b)^2, \quad H_3(Z) = Z(Z/b - 1)/2b$$

$$L_1(Z) = (1 + Z/a)/2, \quad L_2(Z) = (1 - Z/a)/2$$

where  $a = 3^{-1/2}$ ,  $b = 1$  and the locations of  $i$  and  $j$  are shown in Fig. 2. Thus  $\bar{\gamma}_{\xi\zeta}$  and  $\bar{\gamma}_{\eta\zeta}$  have the form suggested by (3). The six unknown parameters for  $\bar{\gamma}_{\xi\zeta}$  are the values  $\bar{\gamma}_{\xi\zeta}^{ij}$  ( $i = 1 \sim 3, j = 1 \sim 2$ ) at the two Gauss point locations ( $\xi = \pm a$ ) on the three lines  $\eta = b, \eta = 0$  and  $\eta = -b$ . Thus  $\bar{\gamma}_{\xi\zeta}$  is linear in  $\xi$  and quadratic in  $\eta$ . Similarly, the six unknown parameters defining  $\bar{\gamma}_{\eta\zeta}$  are the values  $\bar{\gamma}_{\eta\zeta}^{ij}$  ( $i = 1 \sim 3, j = 1 \sim 2$ ) on the two Gauss point locations ( $\eta = \pm a$ ) on the three lines  $\xi = b, \xi = 0$  and  $\xi = -b$ . Thus  $\bar{\gamma}_{\eta\zeta}$  is linear in  $\eta$  and quadratic in  $\xi$ .

2.3 Enhanced Interpolation of The Membrane Strains

In shells, the stiffness associated with the membrane strain energy, though important, especially when the shell thickness becomes very small, should not dominate the total stiffness, The membrane strains can only be separated from the bending strains in the local Cartesian coordinate system. Therefore it is expected that the use of an enhanced interpolation of the membrane strains in the local Cartesian coordinate system can help to eliminate Locking behaviour.

Using analogous method, it is deduced that the values of the membrane strain at lines  $\eta = \pm a$  and  $\xi = \pm a$  (where  $a = 3^{-1/2}$ ) give the best representation of the membrane strain field in each element.

Therefore, in the orthogonal curvilinear coordinate system, the enhanced interpolation for  $e_{m-r}$  and  $\frac{1}{2}e_{m-r}^{(a)}$  is the same as that for  $\gamma_{\xi\zeta}$  and the enhanced interpolation for  $e_{m-r}$  and  $\frac{1}{2}e_{m-r}^{(b)}$  is the same as that for  $\gamma_{\eta\zeta}$ , but they are expressed in different coordinate systems[2].

3. Updated Lagrangian Formulation (U. L.)

In the U. L. formulation, all current static and kinematic variable are referred to the current configuration for each load or time increment step. In the new 9-node degenerated element, the shear and membrane strains have to be interpolated of each iteration and it appears that to use of U. L. formulation is more precise and efficient.

3.1 Equation of Motion[4]

The incremental form of the principle of virtual work based on the U. L. formulation can be written as

$$\int_V {}_t S_{ij} \delta e_{ij} dv + \int_V {}^t \tau_{ij} \delta_r \eta_{ij} dv = {}^{t+\Delta} Q - \int_V {}^t \tau_{ij} \delta e_{ij} dv \quad (5)$$

where  ${}_t S_{ij}$  is second incremental piola-Kirchhoff stresses refered to the configuration at time  $t$ ;  ${}^t \tau_{ij}$  is Cauchy stresses at time  $t$ ;  ${}^{t+\Delta} Q$  is external incremental virtual work at the current load increment. The incremental Green strain is defined as

$$e_{ij} = {}_t e_{ij} + {}_t \eta_{ij}$$

$$e_{ij} = \frac{1}{2} (u_{i,j} + u_{j,i}), \quad \eta_{ij} = \frac{1}{2} (u_{k,i} - u_{k,j})$$

where  $e_{ij}$  and  $\eta_{ij}$  are the linear and quadratic part of  $\epsilon_{ij}$ .

An approximate equation of motion can be obtained by linearization

$$\int_{V'} D_{ijkl} e_{kl} \delta e_{ij} dv + \int_{V'} \tau_{ij} \delta \eta_{ij} dv = {}^{t+\Delta} Q - \int_{V'} \tau_{ij} \delta e_{ij} dv \tag{6}$$

3.2 Constitutive Relations

For considering the large displacement and rotation and large strain, for path-dependent material, following constitutive relations should be used

$$\sigma_{ij}^J = D_{ijkl}^J e_{kl} \tag{7}$$

where  $\sigma_{ij}^J$  are Jaumann stress rate, they are functions only of the deformations of the material and are not affected by rigid body motions. This objective stress rate tensor is defined as

$${}^t\sigma_{ij}^J = {}^t\tau_{ij} - {}^t\tau_{ip} \Omega_{pj} - {}^t\tau_{jp} \Omega_{pi} \tag{8}$$

where  ${}^t\Omega_{ij}$  are incremental spin tensor

$${}^t\Omega_{ik} = \frac{1}{2} ({}^t u_{k,L} - {}^t u_{L,k})$$

The constitutive tensor  $D_{ijkl}^J$  is same as the tensor in the small deformation conditions. with eq. (8), it follows that

$${}^tD_{ijkl} = D_{ijkl}^J - {}^t\tau_{ik} \delta_{jl} - {}^t\tau_{jk} \delta_{il} + {}^t\tau_{ij} \delta_{kl} \tag{9}$$

In eq. (9), the last term represent the effect of elastic volume increment. in general, the elastic strains are far small than the plastic strains, so the last term in eq. (9) may be negligible and it will cause the symmetrization of tensor  ${}^tD_{ijkl}$ .

For isotropic hardening materials, the tensor  $D_{mnl}^J$  can be expressed as

$$D_{mnl}^J = D_{mnl}^e - D_{mnl}^{ep} \tag{10}$$

where

$$D_{mnl}^e = 2G(\delta_{mk}\delta_{nl} + \frac{\nu}{1-2\nu}\delta_{mn}\delta_{kl})$$

$$D_{mnl}^{ep} = \begin{cases} \frac{{}^t\tau_{mn} {}^t\tau_{kl}}{(1/9)(\sigma_e^2/G)(3G + E^p)} & \text{(for loading plastically)} \\ 0 & \text{(for loading elastically and unloading)} \end{cases}$$

in which  ${}^t\tau_{mn}$  are deviatoric components of Cauchy stresses and  $E^p$  is strain-hardening modulers obtained from a true stress-logarithmic strain diagram of the uniaxial material response.

3.3 Finite Element Equations

For the new degenerated shell element, from eqs. (6), the governing finite element equations can be written as

$$({}^tK_L + {}^tK_{NL})\Delta d = {}^{t+\Delta} R - {}^t F \tag{11}$$

where

$${}^tK_L = \int_{V'} {}^t\bar{B}_L^T {}^tD {}^t\bar{B}_L dv \text{---Linear strain incremental stiffness matrix}$$

$${}^tK_{NL} = \int_{V'} {}^t\bar{B}_{NL}^T {}^t\tau {}^t\bar{B}_{NL} dv \text{---Initial stress stiffness matrix}$$

$${}^tF = \int_{V'} {}^t\bar{B}_L^T {}^t\hat{\tau} dv \text{---Vectors of nodal point forces equivalent to the element stresses at time } t$$

in which  ${}^tD$  is constitutive matrix;  ${}^t\tau$  and  ${}^t\hat{\tau}$  are the matrix and vect of Cauchy stresses.

In the eqs. (11), the shear and membrane strains should be interpolated from the values at certain sampling points in different coordinate systems. in general, for shell structures, the large strain is cause by large membrane strain and for this reason the nonlinear term in the shear train can be neglected in the initial stress stiffness matrix.

For dynamic analysis, using implicit time integration, the governing equations may be written as

$$M {}^{t+\Delta} \ddot{d} + ({}^tK_L + {}^tK_{NL})\Delta d = {}^{t+\Delta} R - {}^t F \tag{12}$$

where M is structural mass matrix.

To solve eqs. (12), Newmark's scheme has been adopted.

3.4 Thickness Correction

For a large strain elasto-plastic analysis of shell structures, not only the nodal point coordinates but the thickness of elements should be updated after each loading or time step.

Let  $h_0$  and  $h_1$  are the thickness of a Gauss integration point in the mid-surface of element before and after Loading or time step respectively. The strain increment  $\Delta e'$  along the thickness of element at the integration point can be evaluated by

$$\Delta e' = \frac{1}{2} \sum_{i=1}^m (\Delta e^i w_i) \tag{13}$$

where  $m$  is the number of integration points along the thickness,  $\Delta e^i = \Delta e_x^i + \Delta e_y^i$  and  $w_i$  are weighting factors.

On the basis of the plastic incompressibility condition, the thickness at the integration point,  $h_1$ , can be updated by

$$h_1 = h_0(1 - \Delta e^i) \quad (14)$$

after each loading or time step.

At last, the thickness of integration points are extrapolated to get the value of nodal thickness via the shape function.

#### 4. Numerical Examples

Some examples are now shown to illustrate the accuracy of the present formulation.

##### 4.1 Simply Supported Plate

A simple supported square plate with side length  $L=254\text{mm}$ , thickness  $h=12.7\text{mm}$  and the material density  $\rho=2.825 \times 10^{-9}\text{N} \cdot \text{s}^2/\text{mm}^4$  is subjected to a suddenly applied uniformly distributed load of 2.11MPa. An isotropic material properties is considered:

$$E = 70370\text{MPa}, \nu = 0.3$$

In the calculations, 70 time steps and total time 1.56ms are adopted. Due to symmetry, a quadrant of the plate is discretised  $4 \times 4$  meshes. The central deflection time history for perfect plastic plate with three different yield stresses as well as elastic plate are shown in Fig. 3. As was expected the elastic numerical solution coincide well with the theoretic results and the elasto-plastic solution go up faster with the decrease of yield stresses.

The state of yielding for the outer layer of plate and  $\sigma_T = 210\text{MPa}$  at  $t=1.0\text{ms}$  is shown in Fig. 4.

##### 4.2 Shallow Thin Spherical Cap

A clamped shallow thin spherical cap is subjected to a distributed step pressure of 4.22MPa. The radius of curvature of the shell  $R=576.58\text{mm}$ , thickness  $t=10.41\text{mm}$  and half angle  $\alpha=26.67^\circ$ . The material is assumed to obey the Von Mises yield condition with linear isotropic hardening and  $\rho=2.672 \times 10^{-9}\text{N} \cdot \text{s}^2/\text{mm}^4$ ,  $E=73888\text{MPa}$ ,  $\nu=0.3$ , hardening parameter  $H' = 1478\text{MPa}$ .

100 time steps and time increment  $\Delta t=1 \times 10^{-2}\text{ms}$  are used. The results for elastic and elasto-plastic dynamic analysis are given in Fig. 5. As shown, for this problem the effect of large strain is appeared.

##### 4.3 Deep Thin Spherical Cap

A clamped deep thin spherical cap with a central angle  $\alpha=120^\circ$ , radius  $R=508\text{mm}$  and thickness  $t=7.62\text{mm}$  is subjected to a suddenly applied pressure load of 4.22MPa. The material is isotropic;  $\rho=7.8 \times 10^{-9}\text{N} \cdot \text{s}^2/\text{mm}^4$ ,  $E=2.1 \times 10^5\text{MPa}$ ,  $\nu=0.3$ ,  $H' = 2100\text{MPa}$ . In a quadrant of the shell, 12 elements are used.

The results for elastic and elasto-plastic dynamic analysis are shown in Fig. 6. In the calculation, 100 time step and  $\Delta t=1 \times 10^{-2}\text{ms}$  are adopted.

#### 5. Conclusions

A program for large strain elasto-plastic transient dynamic analysis of shell structures has been developed. For a large strain problem, a more precise results can be obtained with the program. The new degenerated element is capable of analyzing the shock absorber that can absorb the shock energy in form of large plastic strain to lessen the dynamic loading on the vessel.

#### References

- [1] Zienkiewicz, O. C., Taylor, R. L. and Too, J. M., (1971). Reduced Integration Technique in General Analysis of Plates and Shells, Int. J. Num. Meth. Eng., Vol. 3, pp. 275—290.
- [2] Huang, H. C., (1989). Static and Dynamic Analyses of Plates and Shells, London, Springer-Verlag.
- [3] Huang, H. C. and Hinton, E., (1984). A Nine Node Lagrangian Mindlin Plate Element With Enhanced Shear Interpolation, Eng. Comput., Vol. 1, pp. 369—379.
- [4] Bathe, K. J., (1982). Finite Element Procedures in Engineering Analysis, Prentice-Hall, Englewood Cliffs, NJ.

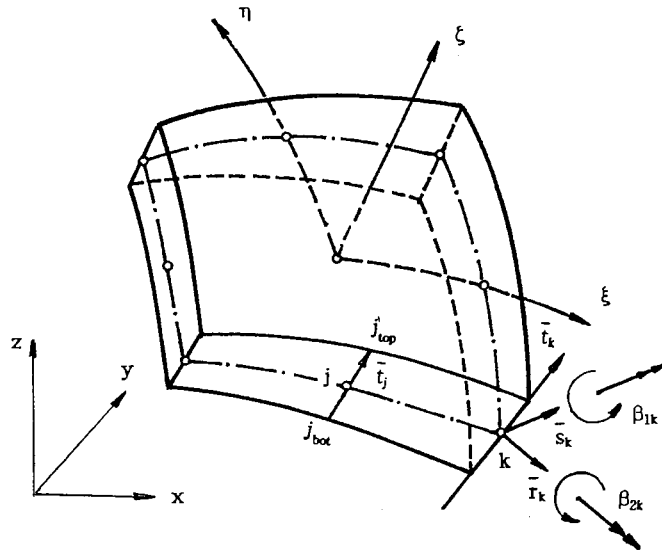


Fig. 1 Quadratic degenerated shell element

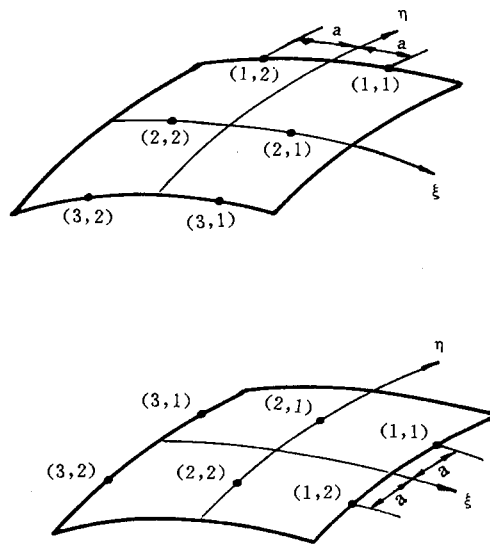


Fig. 2 Interpolation points  $(i, j)$

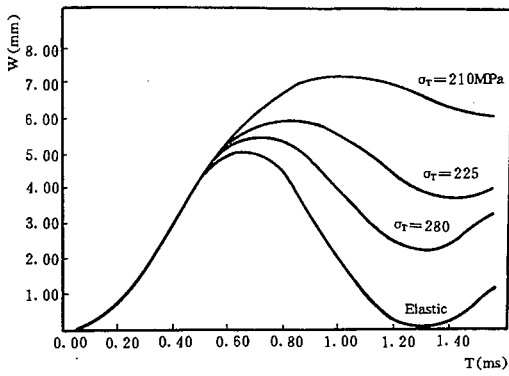


Fig. 3 Central deflection time history for a simply supported square plate

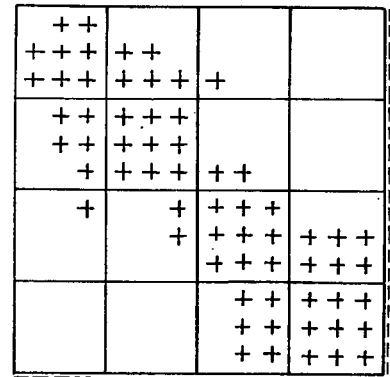


Fig. 4 The distribution of Gause points where the materials have yielded

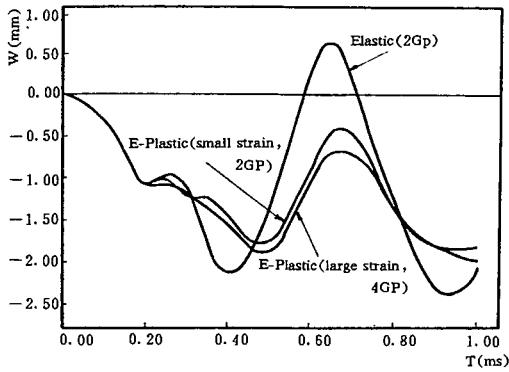


Fig. 5 Central deflection time history for a clamped shallow thin spherical cap

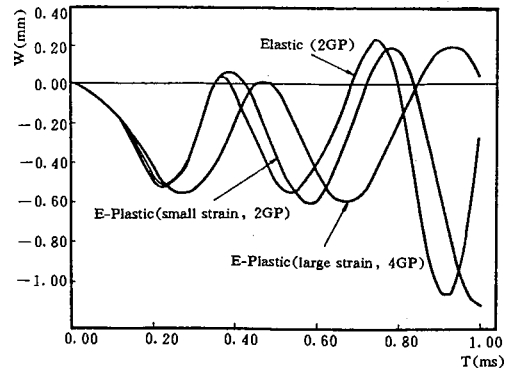


Fig. 6 Central deflection time history for a clamped deep thin spherical cap